LANGMUIR

Article

pubs.acs.org/Langmuir

Sponge Phases and Nanoparticle Dispersions in Aqueous Mixtures of Mono- and Diglycerides

Maria Valldeperas,[*,†] Małgorzata Wiśniewska,[‡,§] Maor Ram-On,[⊥,¶] Ellina Kesselman,[¶,#] Dganit Danino,[¶,#] Tommy Nylander,[†,▽] and Justas Barauskas[‡,○]

[†]Department of Physical Chemistry, Lund University, P.O. Box 124, SE-22100 Lund, Sweden

[‡]Biomedical Science, Faculty of Health and Society, Malmö University, P.O. Box 124, SE-20506 Malmö, Sweden

[§]Department of Chemistry, University of Bergen, P.O. Box 7803, 5020 Bergen, Norway

[⊥]Department of Chemical Engineering, [¶]Russell Berrie Nanotechnology Institute (RBNI), and [#]Department of Biotechnology and Food Engineering, Technion, Israel Institute of Technology, 32000 Haifa, Israel

[▽]NanoLund, Lund University, P.O. Box 118, SE-22100 Lund, Sweden

[○]Camurus AB, Ideon Science Park, Gamma Building, Sölvegatan 41, SE-22379 Lund, Sweden

Supporting Information

ABSTRACT: The lipid liquid crystalline sponge phase (L_3) has the advantages that it is a nanoscopically bicontinuous bilayer network able to accommodate large amounts of water and it is easy to manipulate due to its fluidity. This paper reports on the detailed characterization of L_3 phases with water channels large enough to encapsulate bioactive macromolecules such as proteins. The aqueous phase behavior of a novel lipid mixture system, consisting of diglycerol monooleate (DGMO), and a mixture of mono-, di- and triglycerides (Capmul GMO-50) was studied. In addition, sponge-like nanoparticles (NPs) stabilized by Polysorbate 80 (P80) were prepared based on the DGMO/GMO-50 system, and their structure was correlated with the phase behavior of the corresponding bulk system. These NPs were characterized by dynamic light scattering (DLS), cryo-transmission electron microscopy (Cryo-TEM) and small angle X-ray scattering (SAXS) to determine their size, shape, and inner structure as a function of the DGMO/GMO-50 ratio. In addition, the effect of P80 as stabilizer was investigated. We found that the NPs have aqueous pores with diameters up to 13 nm, similar to the ones in the bulk phase.

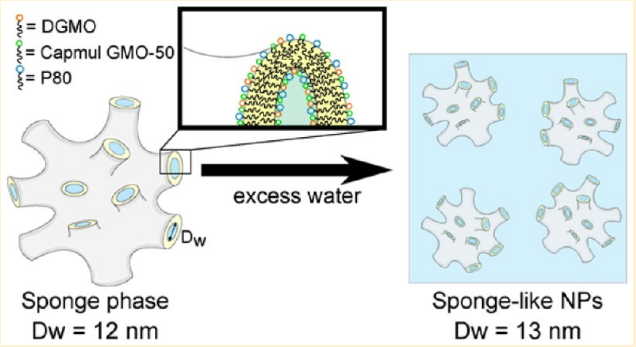

INTRODUCTION

The aqueous phase behavior of unsaturated mono- and diacylglycerols has importance for applications in a variety of fields such as the food industry, biotechnology, and drug delivery.[1−3] Inverted lipid structures are of great interest as they form spontaneously in excess aqueous solutions, which also occur in living organisms.[4−6] Several types of inverted liquid crystalline (LC) phases can exist depending on the lipid composition, including bicontinuous cubic (V_2), hexagonal (H_2), cubic micellar (I_2), sponge phases (L_3), and a variety of intermediate structures with other nonlamellar arrangements.[7]

The most studied unsaturated monoglyceride is glycerol monooleate (GMO), which, depending on temperature, in excess water self-assembles into a reversed bicontinuous Q^{224} cubic or a reverse hexagonal phase.[8,9] However, the possibility to form different LC phases from a single component mono- or diacylglycerol is very limited. Therefore, mixtures of two or more lipids, each of which separately forms different LC phases, can be employed in order to tune the phase behavior.[10−13] The use of a two or multicomponent system can be used to compensate unwanted phase changes caused by guest active compounds that are encapsulated or by external factors, simply by adjusting the ratio of the lipid building blocks, as it was shown in recent studies.[10,14]

In principal, all of these reversed mesophases in excess aqueous solutions can be dispersed into colloidal particles that can be used as drug vehicles for therapeutically active substances.[15−17] Many bulk LC phases and their nanoparticles with reversed cubic and hexagonal nanostructure have been thoroughly investigated.[14,18] However, in certain applications, such as drug delivery,[17,19−21] protein encapsulation or crystallization[22−24] or electrochemical biosensors,[25] where less rigid micro- and nanostructure with large aqueous pores are preferred, there is a lack of knowledge on the structure and size of the pores that limits the use of V_2, L_3, and H_2 bulk phases and dispersions.

Received: April 11, 2016
Revised: August 2, 2016
Published: August 2, 2016

DOI: 10.1021/acs.langmuir.6b01356
Langmuir 2016, 32, 8650−8659

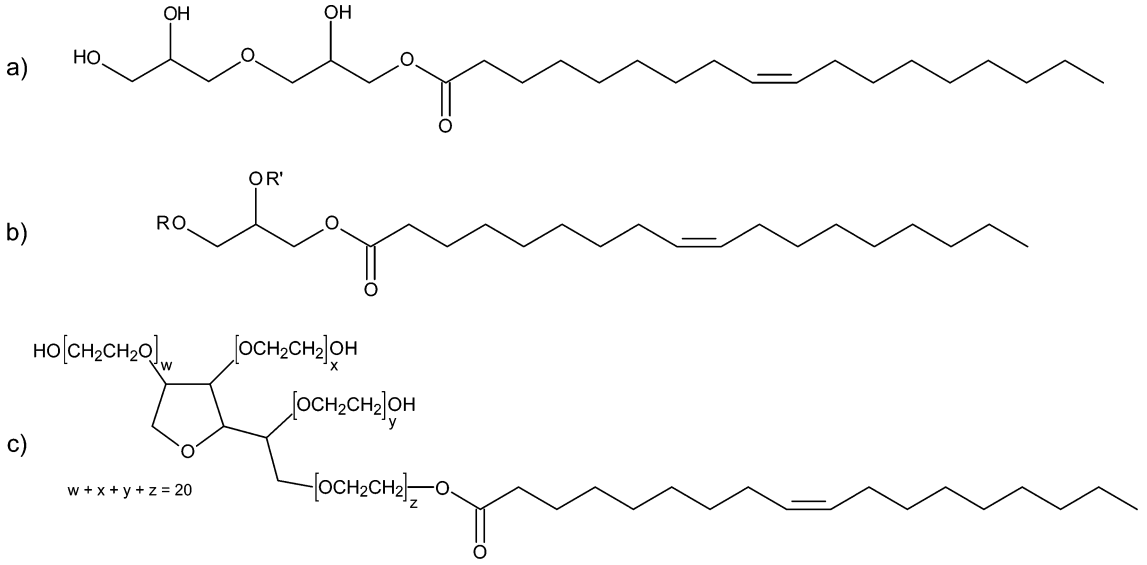

Figure 1. Most predominant molecular structures of (a) diglycerolmonooleate (DGMO); (b) Capmul GMO-50 composed by 54.7% monoglycerides (R = R′ = H); 15−35% diglycerides (R= oleic acid; R′= H); and 2−10% triglycerides (R = R′ = oleic acid); and (c) polysorbate 80 (P80).

Here, the use of a sponge phase that possesses flexible three-dimensional nanostructure with relatively large aqueous pores is particularly favorable. In the phase diagrams, the L_3 phase is usually found in a narrow region between L_α and V_2 phases and represents "melted" cubic phase structure without long-range order.[26] In monoglyceride-based systems it is usually formed by adding organic solvents such as propylene glycol,[27,28] polyethylene glycol,[27,28] ethanol[28] or chloroform.[29] Other examples include mixtures with polymeric compounds, for example in the glycerol monoolein/pluronic F127[30] and glycerol diolein/diglycerol monoolein/polysorbate 80 (P80) systems.[31] The latter system is an interesting example of spontaneous colloidal dispersion formation in a phase region where two liquid phases, L_2 and L_3, coexist with water. However, to our best knowledge the formation of the L_3 phase in simple mixtures of mono- and diglycerides without additional organic solvents has not been previously demonstrated.

As mentioned above, the sponge phase is of great interest due to its ability to form large water pores. The search for highly swollen reverse bicontinuous cubic phase has received more attention recently, especially for the crystallization and immobilization of proteins. Sun et al.[32] achieved cubic water channel diameters up to 7.2 nm by mixing monoglyceride and sucrose stearate. This system was used to immobilize horseradish peroxidase (~6 nm) for biosensing purposes. Another interesting lipid system is the one reported by Tyler et al.[29] Their system consists of a mixture of monoolein, 5 mol % of dioleoylphosphatidylserine (DOPS), and 30 mol % of cholesterol, which forms cubic phases with aqueous pores up to 24.9 nm of diameter at 35 °C.

In this study we demonstrate that a highly swollen L_3 phase can be formed by adding a nonionic polymer, P80, to a mono- and diglyceride-based system without the use of any organic solvent at room temperature (≈ 25 °C). To achieve this, DGMO and Capmul GMO-50 were chosen as the L_α and H_2 phase forming lipid, respectively. In addition, we show that the addition of P80 allows the formation of colloidal stable L_3 phase nanoparticles with narrow and controllable size distribution. Furthermore, these dispersions can be easily prepared without high-energy input, making them easily scalable and promising from the cost-effective point of view.

EXPERIMENTAL SECTION

Materials. A mixture of glycerides denoted as Capmul GMO-50 (Lot No. 100616-8) was provided by Abitec (Janesville, WI). Its composition was 54.7% monoglycerides, 15−35% diglycerides, and 2−10% triglycerides with the following fatty acid composition: 84.6% oleic (C18:1), 6.8% linoleic, 0.8% linolenic, and 6.2% saturated acids. Diglycerol monooleate (DGMO) with 88% of diglycerol monoester and 4.9% free glycerol and polyglycerols was received from Danisco A/S (Brabrand, Denmark). The main fatty acid component was oleic acid constituting 90.7%, followed by linoleic (4.2%), saturated (2.9%), eicosenoic (1.2%), and linolenic (0.8%). Polyoxyethylene (20) sorbitan monooleate (P80) was supplied by Sigma-Aldrich and Croda (Chocques, France) (see Figure 1 for structures). Milli-Q purified water (18 MΩ·cm) was used for all experiments.

Sample Preparation. Lipid mixtures with and without P80 were prepared by weighing appropriate amounts of the compounds into glass vials, which were then left to mix on a roller table for 24 h at room temperature. LC bulk phases were prepared by mixing appropriate amounts of these lipid mixtures with water. The vials were sealed, several times centrifuged up-and-down at 371*g* and left to equilibrate at room temperature for at least 2 weeks before measurements. During equilibration time samples were repeatedly centrifuged up-and-down in order to ensure homogeneity.

Dispersion Preparation. Coarse sponge nanoparticle dispersions were prepared by adding the lipid mixture with P80 to water at a concentration of 5 wt % (lipids+P80) in a 100 mL glass bottle. The total volume of dispersion was 50 mL. The samples were immediately sealed, vigorously hand-shaken and left for 24 h on a mechanical shaking table at 350 rpm and room temperature. To reduce the amount of metastable vesicular aggregates, a heat-treatment procedure was performed at 121 °C and 1.4 bar for 36 min (Prestige Medical Classic 2100 Autoclave, TG-Instrument AB, Helsingborg, Sweden).

Small Angle X-ray Scattering (SAXS). SAXS measurements were performed at the I911-4 SAXS beamline at MAX-Lab (Lund University, Sweden). The scattered intensity was recorded at room temperature (25 °C ± 0.1 °C) using a wavelength of 0.91 Å and a Pilatus 1 M 2D detector at a sample-to-detector distance of 1913 mm. Bulk LC samples were mounted between kapton windows in a steel sample holder, whereas dispersions were filled into quartz capillaries. The exposure time for LC phases and their dispersions was 60 and

DOI: 10.1021/acs.langmuir.6b01356
Langmuir 2016, 32, 8650−8659

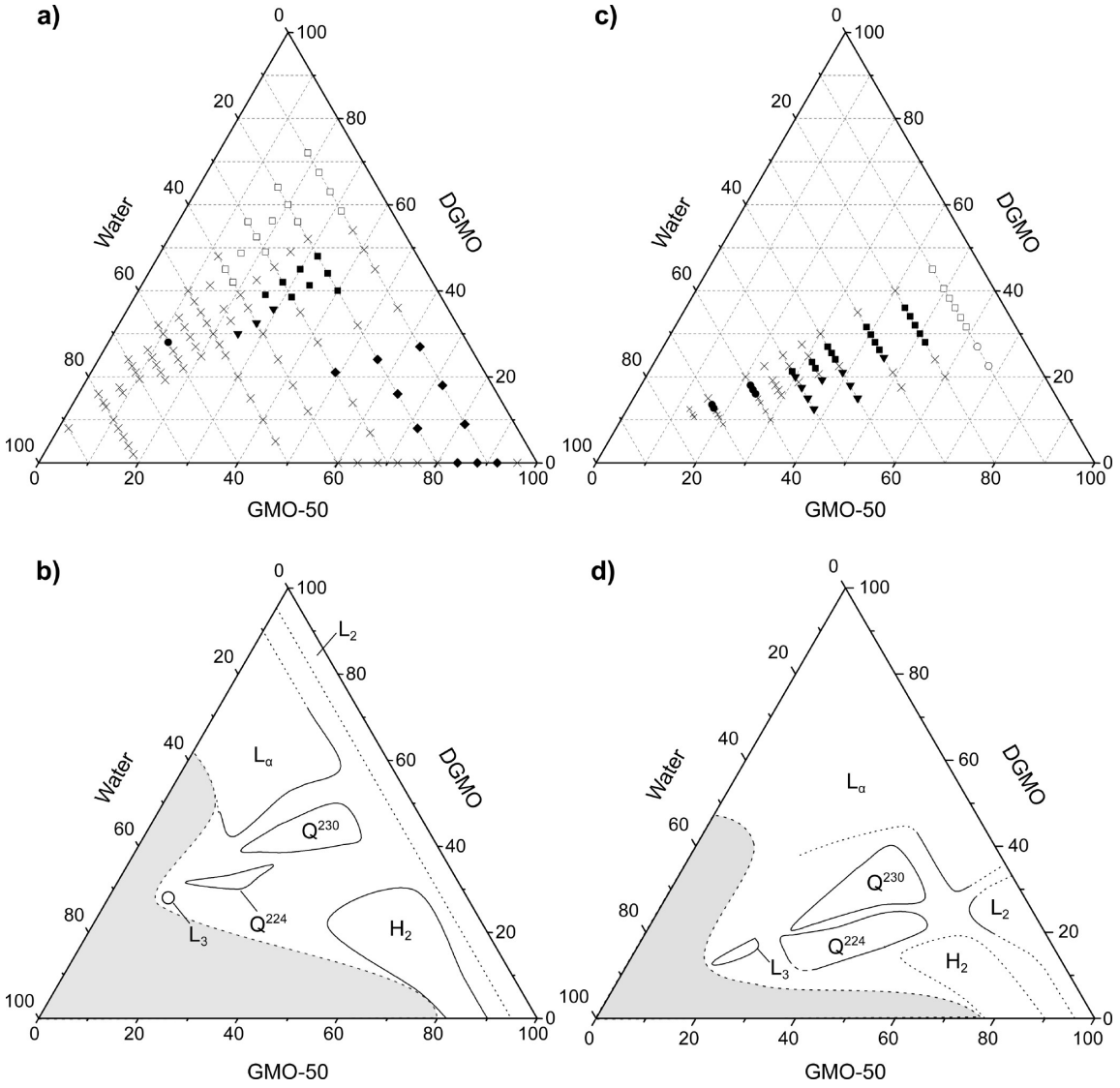

Figure 2. Investigated samples used to construct the ternary DGMO/GMO-50/water (a) and pseudoternary DGMO/GMO-50/P80/water phase diagram (c), and the resulting schematic phase diagram (b and d, respectively). Symbols denote L_α (open squares), Q^{230} (filled squares), Q^{224} (filled triangles), L_3 (filled circles), H_2 (filled diamonds), L_2 (open circles), and multiple phase mixtures (crosses). Gray areas indicate the observed and predicted water excess regions. Solid lines show determined one phase region, and dashed lines show the expected phases. Note that DGMO and GMO-50 compositions were adjusted for sake of clarity, as the lipid/P80 ratio was kept constant for all the samples. Phases were determined by SAXS and/or visual inspection under cross polarizers (see Figure S1).

60−300 s, respectively. The two-dimensional SAXS patterns were analyzed using the Fit2D software. Silver behenate was used as a reference to calibrate sample-to-detector distance and detector positions.

Bulk LC phases were also measured using the SAXSLab Ganesha 300XL instrument (SAXSLAB ApS, Skovlunde, Denmark). The instrument was equipped with a 2D 300 K Pilatus detector from Dectris and a Genix 3D X-ray source. The X-ray wavelength was 1.54 Å and the data were collected in the q range of 0.013−0.76 Å^{-1}. Samples with low water content were sealed at room temperature between two thin mica windows in a metallic block, whereas the other ones (60−70% water) were filled into quartz disposable capillaries (Hilgenberg GmbH, Malsfeld, Germany). Exposure times varied from 30 to 60 min. In all cases, the temperature was kept at 24 ± 0.2 °C by an external recirculating water bath. The two-dimensional scattering pattern was radially averaged using SAXSGui software to obtain $I(q)$. Some experiments were also performed on a Kratky compact SAXS system (OED 50 M from MBraun, Graz, Austria) as described in the literature.[31]

Estimation of Water Channel Dimensions. The obtained X-ray diffraction data were applied to estimate the water channel radius (r_w) of reverse cubic phases in the DGMO/GMO-50/P80/water system. The d-spacing ($d = 2\pi/q$) obtained from SAXS and the volume fraction of the nonpolar part (see SI for equation and density values) were used to calculate the monolayer thickness. For this purpose, it was considered that reverse cubic phases are curved lipid bilayers draped onto an infinite periodic minimal surface (IPMS), located at the middle of the bilayer. According to this model, the monolayer on each side of the midplane has a constant thickness, l, which can be calculated by solving[33,34]

$$\Phi_{\mathrm{lip+P80}} = 2A_0\left(\frac{l}{a_{\mathrm{cub}}}\right) + \frac{4\pi\chi}{3}\left(\frac{l}{a_{\mathrm{cub}}}\right)^3 \quad (1)$$

where A_0 is the ratio of the IPMS area to (unit cell volume)$^{2/3}$ and χ is the Euler−Poincaré characteristics. These parameters are defined by the cubic space group (see values in Table S1). The inverse of the experimentally obtained lattice parameters (a_{cub}) were plotted as a

DOI: 10.1021/acs.langmuir.6b01356
Langmuir 2016, 32, 8650−8659

function of lipid volume fraction for the cubic phases in order to find from the slope the monolayer thickness value.

Then, the molecular cross-sectional area at a distance ξ from the IPMS and integrated over one of the two monolayers within the unit cell $A(\xi)$, was calculated as follows:[34,35]

$$A(\xi) = A_0 {a_{cub}}^2 + 2\pi\chi\xi^2 \quad (2)$$

With eq 2 the radius of the water channel (r_w) for the cubic phases was estimated, as $A(\xi)$ reduces to zero at the center of the water channel and then, ξ is the sum of l and r_w. By making appropriate substitutions, eq 2 reduces to[35]

$$r_{w-cubic} = -\left(\frac{A_0}{2\pi\chi}\right)^{1/2} a_{cub} - l \quad (3)$$

To estimate the r_w of the sponge phase, the quotient ($y_{L_3/cub}$) between the d-spacing of the sponge phase (d_{L_3}) and the previous cubic phase (d_{cub}) was calculated as follows:

$$y_{L_3/cub} = d_{L_3}/d_{cub} \quad (4)$$

The values of the first peak for both phases and the same DGMO/GMO-50 ratio were used, and then, the water channel radius of the cubic phase was multiplied by $y_{L_3/cub}$ to obtain the sponge phase r_w.

Dynamic Light Scattering (DLS). The particle size and size distribution were measured by dynamic light scattering (Zetasizer Nano ZS, Malvern Instruments Ltd., Worcestershire, UK), using disposable cuvettes filled with 1 mL of 0.5 wt % nanoparticle dispersion at 25 °C. Data were collected after 2 min equilibration time and averaged over three measurements. The refractive indexes used for lipid particles and water were 1.48 and 1.33, respectively. The apparent hydrodynamic radius was thereafter calculated using the Stokes–Einstein relation assuming spherical particles. The particle size distributions were characterized by intensity averaged mean and polydispersity index, PdI.

Cryogenic-Transmission Electron Microscope (Cryo-TEM). Cryo-TEM samples were prepared in the controlled environment vitrification system (CEVS) or the Vitrobot (FEI, The Netherlands) at 25 °C, and at 100% relative humidity to prevent evaporation from the specimen. Prior to specimen preparation, the grids were plasma etched in a PELCO EasiGlow glow-discharger (Ted Pella Inc., Redding, CA) to increase their hydrophilicity. In the specimen preparation chamber, a carbon-coated perforated polymer film, supported on a 200 mesh TEM grid was held by tweezers. A drop of the sample was placed on the film, and blotted to form a thin film of liquid. The specimen was then vitrified by quickly plunging into liquid ethane at its freezing point. After vitrification the sample was kept in liquid nitrogen until transfer into the TEM for imaging. Imaging was performed using an FEI Tecnai T12 G^2 transmission electron microscope. The microscope is equipped with LaB6 electron gun and operates at 120 kV. Specimens were equilibrated in the microscope below −178 °C in Gatan 626 cryo-holders, and imaged using a low-dose imaging procedure to minimize electron-beam radiation-damage. Images were recorded on a Gatan US1000 high-resolution cooled-CCD camera, using the DigitalMicrograph software package, as previously described.[36,37]

Cryogenic-Scanning Electron Microscope (Cryo-SEM). Specimens were prepared in a controlled environment vitrification system (CEVS) at 25 °C and 100% humidity. A drop of the solution was sandwiched between two gold planchettes, held by special tweezers. The tweezers were then rapidly plunged into liquid nitrogen at its boiling point, and the sandwich was inserted into a "sample-table" also cooled in liquid nitrogen. The sample-table was then transferred into a BAF060 freeze–fracture–replication system, a high vacuum system, where it was set on a cooled stage at −175 °C. The sandwiches were split open to fracture the frozen specimen. The specimens were then transferred under vacuum and cryogenic temperature by a BalTec VCT100 shuttle, precooled with liquid nitrogen, to the precooled cryo-stage of the HR-SEM for imaging. The sample was also prepared with liquid ethane in order to rule out artifacts and check that the same nanostructure was obtained (images not shown).

RESULTS AND DISCUSSION

Phase Behavior of DGMO/GMO-50/Water System. The phase behavior of the ternary system DGMO/GMO/water has been previously studied by Pitzalis et al.[11] This system exhibits lamellar phase up to 20 wt % of water content in the GMO/water axis, followed by the cubic phases with space group *Ia*3*d* and *Pn*3*m*, which swell up to around 50 wt % of aqueous solvent. Adding DGMO to the GMO/water system increases the swelling limit because of the enlarged polar headgroup volume caused by a second glycerol group in the DGMO structure. Here we used Capmul GMO-50 (GMO-50) instead of pure GMO to promote the formation of swollen reverse structures. The phase behavior of the DGMO/GMO-50/water system was mapped by preparing samples with different fixed lipid ratios and diluted with different amounts of water to cover the entire phase diagram. GMO-50/water mixtures with increasing DGMO content have been formulated with DGMO/GMO-50 ratios from 10/90 to 80/20.

Five different phases surrounded by mixed phase areas were identified by X-ray diffraction and visual inspection under polarized light, as indicated in Figure 2a,b. In the GMO-50/water axis the reversed hexagonal phase (H_2) is distinguished in the range of 6–18 wt % of water. This is based on the observed birefringence between crossed polarizers and Bragg peaks following the ratio of $1:\sqrt{3}:\sqrt{4}:\sqrt{7}:3$. The H_2 phase is extended in the ternary DGMO/GMO-50/water system up to a DGMO/GMO-50 ratio of 30/70. With increasing DGMO concentration the swelling limit for the H_2 increases from 16 wt % to around 36 wt % water.

As DGMO content is increased, a narrow region of a rigid isotropic phase is observed from the DGMO/GMO-50 ratio of 50/50. SAXS diffraction patterns obtained from these samples indicate that there are two reverse bicontinuous cubic structures in this region. Between 20 and 35 wt % of water, eight Bragg reflections at the spacing ratios $\sqrt{6}:\sqrt{8}:\sqrt{14}:\sqrt{16}:\sqrt{20}:\sqrt{22}:\sqrt{24}:\sqrt{26}$ are observed, which correspond to a cubic phase with *Ia*3*d* space group (Q^{230}). At a higher degree of hydration, the Q^{230} phase transforms into another cubic phase. This phase expands from 35 wt % up to 45 wt % of water in the dilution line of 55/45 DGMO/GMO-50 and shows eight Bragg peaks with relative position in ratios $\sqrt{2}:\sqrt{3}:\sqrt{4}:\sqrt{6}:\sqrt{8}:\sqrt{9}:\sqrt{10}:\sqrt{11}$, which are the reflections of the *Pn*3*m* space group (Q^{224}).

A narrow and well-defined area of an isotropic and fluid phase is found when moving from *Pn*3*m* phase toward higher DGMO and water content (Supporting Information, Figure S1c). The diffractogram features two diffuse Bragg peaks that correspond to the L_3 sponge phase, which seems to be strongly linked to the previous cubic phase (Figure S2). In fact, a multiphase region exists between the cubic and sponge phase, where the cubic Q^{224} is predominant (Figure S1b). Further increasing of water content shows the coexistence of the sponge phase with excess water (Figure S1d,e), whereas coexistence with L_α is found at higher DGMO contents. Thus, the location of the L_3 phase in the phase diagram as explained above, its fluidity, and its SAXS profile enable us to unambiguously identify it as an L_3 phase and not an L_2.

If we move from the region of cubic phases and increase the DGMO content, we discover the lamellar phase (L_α). This phase shows three strong Bragg peaks with the spacing ratio of

DOI: 10.1021/acs.langmuir.6b01356
Langmuir 2016, 32, 8650–8659

1:2:3 and exhibits birefringent behavior when observed through crossed polarized light. The swelling limit of this phase is higher than 40 wt % of water when the DGMO/GMO-50 ratio was 70/30, as this phase is coexisting with a bicontinuous cubic phase at 50 wt % water (Figure S1a), and up to 40 wt % for the other compositions studied with high DGMO content. This behavior agrees with the literature[11,38] in which L_α is formed with the swelling limit of around 40 wt % of water at high DGMO concentrations.

A comparison of the investigated system with the one described by Pitzalis et al.[11] makes it easy to notice the difference in the phase behavior. The above-mentioned dissimilarities between DGMO/GMO/water and DGMO/GMO-50/water systems are related mainly to the GMO-50 composition, which although comprises mostly glycerol monooleate contains noticeable amounts of di- and triglycerides. These compounds entail the lower degree of hydration compared to the binary pure GMO/water system and enhance the formation of phases with more negative spontaneous curvature, such as the reverse hexagonal phase.

Phase Behavior of DGMO/GMO-50/P80/Water System. Samples with P80 have been studied in order to swell the sponge and bicontinuous cubic phase region, as well as enlarge their unit cell dimensions. In addition, P80 is a stabilizer used to disperse the DGMO/GMO-50 nonlamellar phases into liquid crystalline nanoparticles. In the present work, the DGMO/GMO-50 ratio has been varied from 25/75 to 50/50, to which P80 has been added at a fixed lipid/P80 ratio of 70/30, and then different amounts of water have been added to cover the whole range of hydrations. All samples were analyzed by SAXS and visual inspection under polarized light. In addition, samples with a 40/60 DGMO/GMO-50 ratio at 60% hydration were observed by Cryo-EM techniques.

Figure 2c,d shows the detailed and schematic phase diagram, respectively, of the DGMO/GMO-50/P80/water system. Note that DGMO and GMO-50 compositions have been adjusted to be able to directly compare the DGMO/GMO-50/P80/water system in terms of the water content, as the lipid/P80 ratio was kept constant for all the samples. For that, the P80 was taken into account in the lipid fraction. At low hydration, lamellar phase (L_α) and reverse micelles (L_2) are present at intermediate and low DGMO content, respectively. L_α exists in samples above the DGMO/GMO-50 ratio of 35/65, showing birefringence under crossed polarizers and two Bragg reflections at the spacing ratios 1:2. L_2 presents a broad peak in the X-ray diffractogram and no birefringence is observed.

Two isotropic cubic phases are found when the water content is increased. A body-centered cubic phase with *Ia*3*d* space group is identified at high DGMO content. Up to eight Bragg peaks are established by X-ray diffraction with the spacing group relationship of $\sqrt{6}:\sqrt{8}:\sqrt{14}:\sqrt{16}:\sqrt{20}:\sqrt{22}:\sqrt{24}:\sqrt{26}$, which corresponds to the Bragg reflections (211), (220), (321), (400), (420), (332), (422), and (431). This phase swells up to 50 wt % of water in the samples with higher DGMO concentration and transforms into the *Pn*3*m* space group at lower DGMO content (around the dilution line of 37.5/62.5 DGMO/GMO-50). The reverse bicontinuous cubic phase with *Pn*3*m* space group extends from 25/75 to 40/60 DGMO/GMO-50 ratio and up to 50 wt % water. At least four Bragg peaks are identified with the relative positions of $\sqrt{2}:\sqrt{3}:\sqrt{4}:\sqrt{6}$, which can be indexed as (110), (111), (200), and (211). This phase is predominant at the lower DGMO and water contents studied, although it coexists with the reverse hexagonal phase (H_2). The characteristic Bragg peaks and stiffness of the Q^{224} phase and the observed birefringence confirm the coexistence of Q^{224} and H_2 phases.

At even higher water content, an isotropic fluid phase is distinguished at DGMO/GMO-50 ratios of 40/60 to 45/55 (as detailed in Figure 2c). Two diffuse peaks are observed in the X-ray scattering pattern, which are characteristic of the L_3 sponge phase. The first maximum corresponds to the L_3 cell−cell correlation distance, whereas the second one is related to lipid bilayer distances.[39−41] Samples surrounding this region also show similar diffuse peaks, although they are in equilibrium with another phase or exist in excess of water. For instance, at 55 wt % water the L_3 phase coexists with inverse bicontinuous cubic phases, mainly *Pn*3*m*. The addition of 5 wt % solvent produces "pure" sponge phases at higher DGMO concentrations and coexistence with excess water at lower DGMO content. The coexistence of the L_3 phase with excess of water was identified using crossed polarizers but also from SAXS data, which showed no shift toward lower *q*-values. An exception of this behavior is the dilution line with 50/50 DGMO/GMO-50, in which L_α is always present and exists with L_3 and water at higher hydrations.

To discard the presence of inverse micelles (L_2) and obtain more detailed characterization of the sponge phase, this phase was studied by cryo-EM techniques as will be discussed later. In addition, a detailed analysis of the scattering data was carried out.

Figure 3 displays the SAXS patterns of the samples with a 40/60 DGMO/GMO-50 ratio as a function of water content.

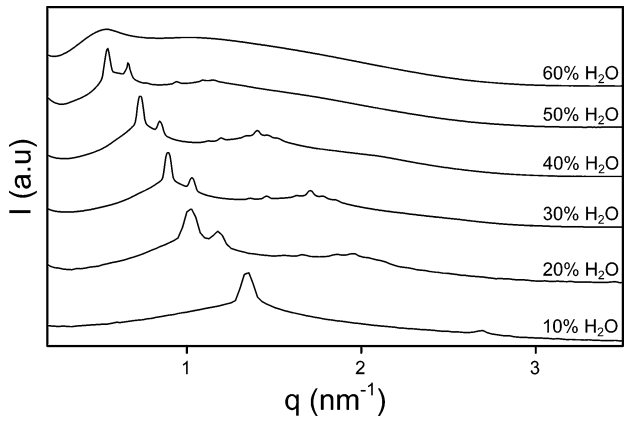

Figure 3. SAXS data of 40/60 DGMO/GMO-50 samples at different degrees of hydrations (wt % water indicated), with constant lipid/P80 ratio of 70/30. Phase transitions from L_α to L_3, through cubic phases, can be noticed.

At this lipid composition, the system is transformed from a lamellar phase to sponge phase, passing through the cubic phases with *Ia*3*d* and *Pn*3*m* space group. Several phase transitions are produced when increasing the amount of water and the peak is shifted toward lower *q*-values. This is the result of increasing the radius of the water channels due to increase uptake of water as will be discussed further below. It is worth noting that the L_3 sponge phase bilayer structure is closely related to the cubic phase that occurs at lower water content, as the main diffuse peak of the sponge phase appears at the same position as the strongest peaks from the Q^{224} (see Figure S3). Therefore, the two diffuse peaks of the L_3 phase are associated with some periodic repeat distances present in this

DOI: 10.1021/acs.langmuir.6b01356
Langmuir 2016, 32, 8650−8659

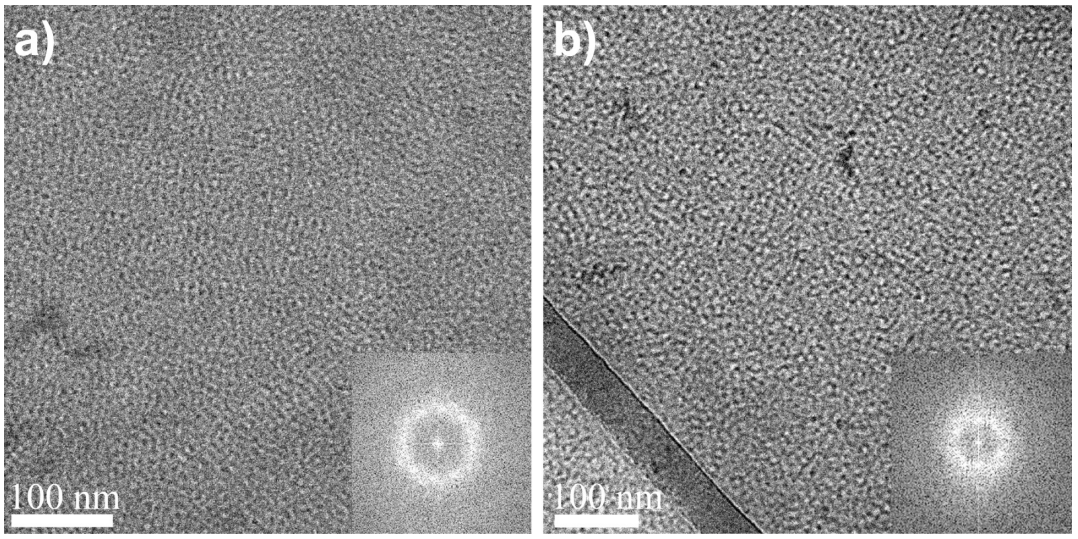

Figure 4. Cryo-TEM images at different magnifications of the 60% hydration bulk phase sample with 40/60 DGMO/GMO-50 and lipids/P80 ratio of 70/30. These images are of different areas of the sample with slightly different magnification. Fast Fourier transformations of images a and b are shown, and analysis represents a *d*-spacing of 11.2 ± 2 nm. The corresponding cryo-SEM image is shown in Figure S4.

phase, as for the cubic phases, which can be related to the aqueous pores radius as will be described below.

To further confirm the presence and morphology of the L_3 phase, we used cryo-TEM and cryo-SEM to image a representative sample (40/60 DGMO/GMO-50 with 60 wt % of water). A highly dense and homogeneous structure is observed in the cryo-TEM images (Figure 4a,b). An important feature of these micrographs is the diffuse order characteristic of the L_3 phase, which has been confirmed by the broad ring on the fast Fourier transformation (FFT) image. FFT analysis of several cryo-TEM micrograph (only two are shown) give a *d*-spacing of about 11.2 ± 2 nm, which corresponds to the *d*-spacing extracted from Figure 3 of 12.7 nm. Here we note that the FFT analysis for this type of flexible structures gives a rather broad distribution of *d*-spacing. Since cryo-TEM micrographs are images of three-dimensional structures projected into a two-dimensional image, topographical features can be challenging to interpret. This type of information can be more clearly provided by cryo-SEM. However, together with the phase behavior of the system and SAXS data, these cryo-EM micrographs support the existence of the sponge phase. In Figure S4 a cryo-SEM micrograph of the freeze-fractured of the corresponding sample is shown. It should be noted that in contrast to cryo-TEM images, this is taken at a 10 times lower magnification and represents the surface topography of a fracture plane of the phase. Even on this length scale the image could be interpreted as some kind of continuous lipid although the resolution does not allow an unambiguous determination of the structure.

A comparison of this system to the DGMO/GMO-50/water system shows that the influence of P80 on the formation of liquid crystalline phases can be easily observed (Figure 2). P80 is a nonionic polymer with an oleic acid chain and a larger polar headgroup compared to DGMO and GMO-50. As a result of its molecular structure (Figure 1c), the packing parameter ($N_s = v/al$) is lower than for the other components thanks to the larger effective size of the headgroup. Thus, this component promotes the formation of structures with lower curvature when mixing with DGMO and GMO-50. This behavior can be clearly noticed by the increase of water uptake for cubic and sponge phases. They can therefore be formed in a higher range of compositions due to the improvement of the swelling properties conferred by the addition of P80.

The enhancement of swelling abilities will be reflected as the increase in the water channel dimensions. SAXS data have here been used for this purpose as described in the Experimental Section. First, the monolayer thickness has been estimated (eq 1) and then, used to calculate the water pore radius, r_w (eq 3).

Fitting of the theoretical swelling law agrees with experimental data (Figure S5) and results in a monolayer thickness value of 2.2 and 2.3 nm for *Ia*3*d* and *Pn*3*m*, respectively. Because of the addition of P80 and the presence of di/triglycerides in GMO-50, monolayer thickness values differ slightly from those reported for the DGMO/GMO/water system, in which distances from the midplane of the bilayer to the neutral surfaces are 1.2 and 1.5 nm for *Ia*3*d* and *Pn*3*m*, respectively.[9]

Figure 5 summarizes the estimated water channel diameter (D_w) as a function of water content for both cubic phases and the sponge phase. As can be seen, D_w increases with addition of water, even though it is rather independent of the DGMO/GMO-50 ratio within the investigated range. In fact, it varies for the cubic phase from 2.8 to 8.4 nm at low and high hydrations, respectively, and reaches values of 12 nm for the L_3 phase (see Table S2). These results support the idea that by adding a nonionic polymer, such as P80, in the DGMO/GMO-50/water system large water channels could be obtained. They also confirm that P80 enters into the LC phase. These results are promising for the entrapment of large molecules, such as proteins or peptides, as the dimensions of the aqueous pores are large enough. Therefore, DGMO/GMO-50/P80/water system is suitable for the encapsulation of molecules up to 12 nm in size and even more if those molecules are able to penetrate into the bilayer.

Dispersions of DGMO/GMO-50/P80/Water System. Nanoparticle dispersions have been prepared with the aim to produce particles with large unit cell dimensions. As reported above, this is possible by adding P80 to the DGMO/GMO-50/water system. Spontaneous dispersions have been formulated at a concentration of lipid and P80 mixtures of 5 wt %, by simply

DOI: 10.1021/acs.langmuir.6b01356
Langmuir 2016, 32, 8650−8659

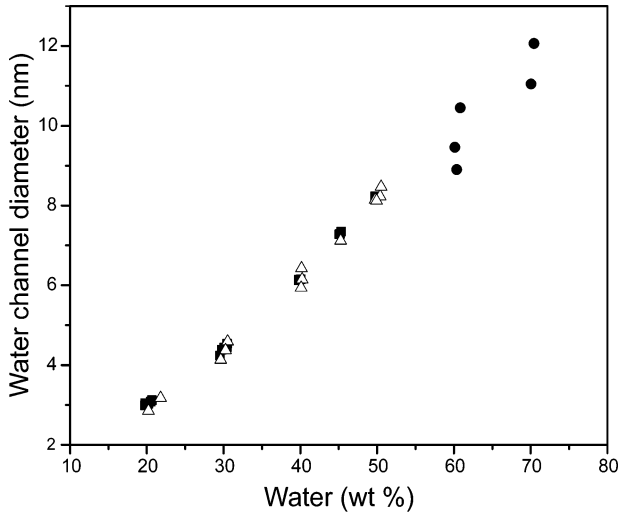

Figure 5. Estimated water channel radius as a function of wt % water for bicontinuous cubic phases Q^{224} and Q^{230} (filled squares and open triangles, respectively) and sponge phase L_3 (filled circles).

shaking the solutions 24 h at 350 rpm. Samples were analyzed by dynamic light scattering, synchrotron X-ray scattering and cryo-TEM.

The average size of nanoparticle dispersions at different DGMO/GMO-50 ratio was determined by DLS before and after the heat treatment. As previously reported,[14,31] this heat process reduces the vesicles present in the dispersion. Indeed, the vesicular structures were found to have fused after heat treatment and the nanoparticles became larger and less polydisperse (Table S3). It is noteworthy that even without the heat treatment the nanoparticles stabilized by P80 have a narrow size distribution. For coarse dispersions, the size grows up to a relative DGMO content of 40 wt %. Further increase in the DGMO concentration on the other hand results in a decrease of the average size although the data are scattered. Such behavior can be explained by the proximity of the sponge-to-lamellar phase transition. At higher DGMO contents the system is close to the lamellar phase and more vesicles and liposomes might be formed. In contrast, after the heat treatment the nanoparticles' tendency is to increase in size with the addition of DGMO. More of these vesicular structures

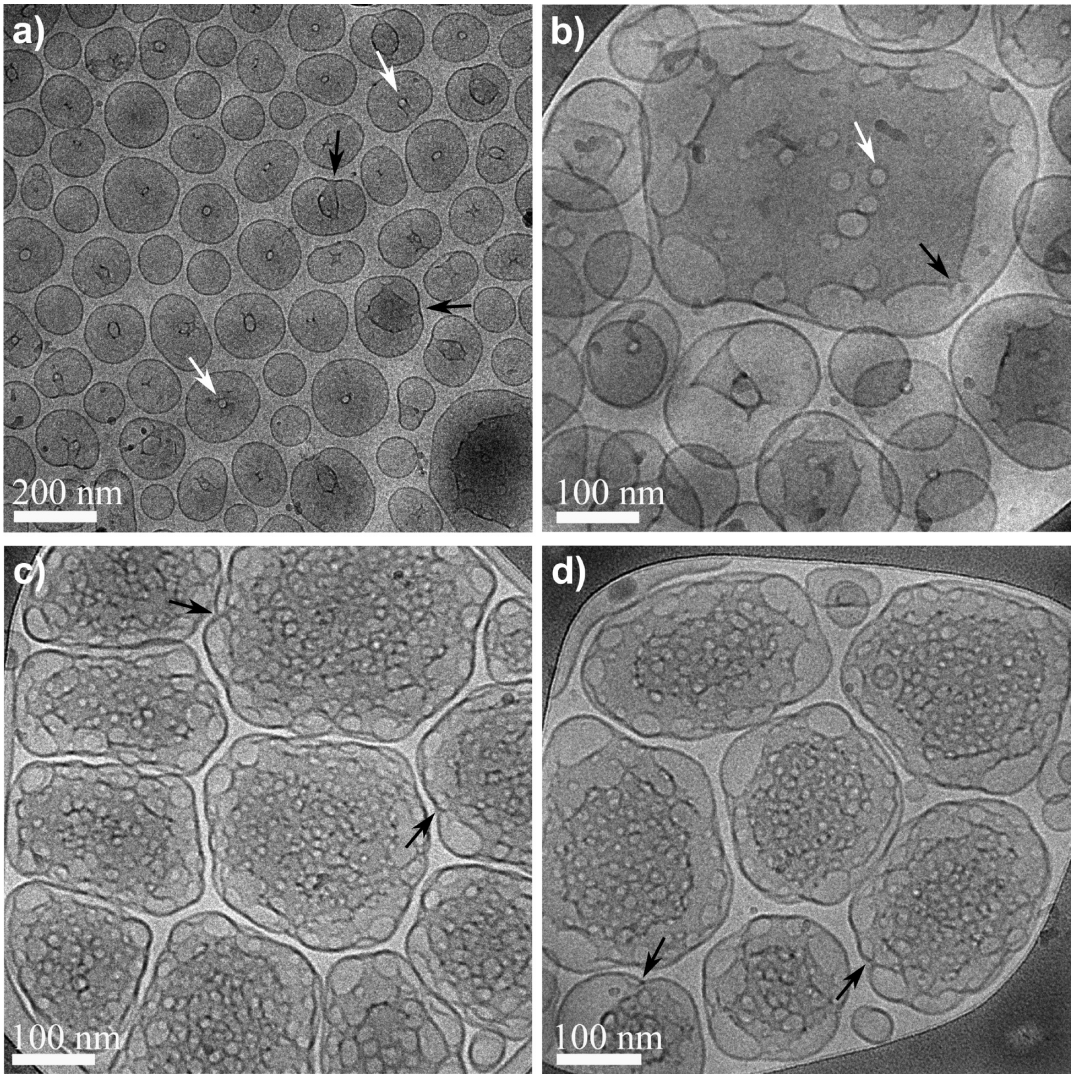

Figure 6. Cryo-TEM images of nanoparticles dispersions with lipid/P80 = 70/30 and DGMO/GMO-50 = 50/50 (a,b) and 40/60 (c,d) at different magnifications. Black and white arrows indicate some interlamellar attachments (ILAs) and aqueous channels formed, respectively.

DOI: 10.1021/acs.langmuir.6b01356
Langmuir 2016, 32, 8650−8659

are expected to have fused with the particles after the heat treatment, which in turn lead to an increase in size.

Two representative dispersions have been chosen to illustrate by cryo-TEM the changes in particle structure by varying the DGMO/GMO-50 ratio. Figure 6 displays well-defined nanoparticles with 50/50 and 40/60 DGMO/GMO-50, respectively. However, they present a very distinct structure. The first one with higher content of DGMO results in nanostructures without apparent inner order mixed with some vesicles (Figure 6a,b). Those nanoparticles feature signs of forming interlamellar attachments (ILAs),[42] which will develop to the pores of sponge-like structure, as can be seen in the larger particles and in the particle dispersion with higher GMO-50 content (Figure 6c,d). This fact agrees with previous work,[43,44] in which it was suggested that inverted bicontinuous cubic phases can be formed from ILAs between opposed bilayers. Therefore, we propose that the L_3 phase is an intermediate between ILAs and the inverse bicontinuous phase. Here the large number of connections between bilayers as well as the curvature promoted by the chosen lipid composition allows the system to form water channels arrays without long-range order (also stated by Efrat et al.[45]).

As the GMO-50 content is increased, more sponge-like nanostructures appear, in agreement with the bulk phase behavior. The micrographs of 40/60 DGMO/GMO-50 nanoparticle dispersion illustrate this feature. As can be seen in Figure 6c,d, these nanostructures show a sponge-like arrangement through the whole particle. This arrangement can be distinguished by the circular features present on the particles, which correspond to the aqueous pores of the L_3 phase.

As can be noticed, the nanostructure of these particles includes more inner and surface defects not present in the bulk phase state, where the L_3 phase structure is homogeneous and infinite through the whole sample. As a result, some structural defects can be noticed by the diversity in size of the water channels (circular features) and the difference in compactness of the L_3 structure. This structure is slightly less dense on the surface region due to the swelling of the bilayer interface structure, where some ILAs can be also observed. This behavior can be attributed to the flexibility of the L_3 bicontinuous bilayer, which in contact with excess water adapts to a more swollen structure. P80 may play an important role here, which due to its large headgroup favors these structures and confers higher stability to the particles by being more concentrated on the surface. These changes might lead to a difference in composition distribution in the inner region of the particle compared to the outer or surface region. This has been previously reported by Wadsäter et al.,[46] who found that P80 stabilizes soy phosphatidylcoline and glycerol dioleate NPs by being more concentrated to the particle surface. However, further studies should be carried out to confirm that P80 behaves in the same way in the system investigated here. If more GMO-50 is added (up to 75 wt % compared to DGMO), nanoparticles with cubic inner structure start to form (data not shown).

In addition to the cryo-TEM, all dispersions have been analyzed by SAXS. Figure 7 illustrates typical scattering data for the above mention dispersions, where the two diffuse peaks characteristic of the L_3 phase could be identified. As can be perceived, the first diffuse peak, which is related to the L_3 cell−cell correlation distance, has a less well-defined maximum compared to the bulk sponge phase due to the distribution in the repeat distances mentioned above. Therefore, the second

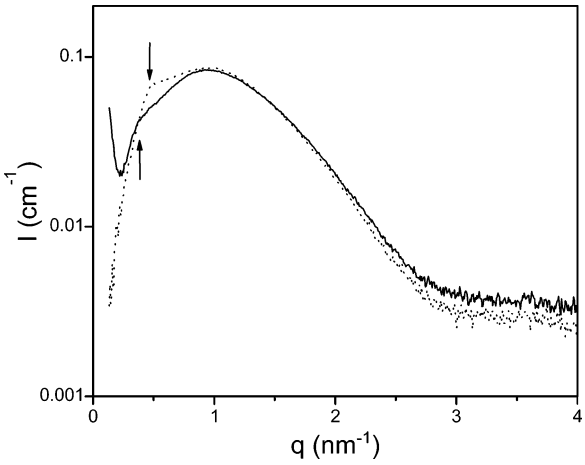

Figure 7. SAXS profiles of nanoparticles dispersions with a DGMO/GMO-50 ratio of 50/50 (straight line) and 40/60 (dot line). Arrows indicate the *q*-values used for estimating the aqueous pore size.

diffuse peak associated with the lipid bilayer distances becomes more visible, as the bilayer thickness remains better defined through the entire sample. As for the bulk phases, the first peak has been used to estimate the water channel diameter, which was found to be up to 13 nm for the 45/55 DGMO/GMO-50 nanoparticles dispersion (see Table S2). It is important to mention that no significant changes in particle size and size distribution have been detected during storage for about three months at room temperature.

CONCLUSIONS

Aqueous phase behavior of a mixture of mono- and diglycerides was studied in the absence and presence of P80. This nonionic polymer enables a change in the spontaneous curvature of the DGMO/GMO-50 lipid bilayer, making it more flexible, more suitable for forming bicontinuous cubic and L_3 phases, and better able to accommodate larger amounts of water. In fact, highly swollen sponge phases have been achieved by simply mixing the components and without the use of any organic solvent.

In addition, we have demonstrated that colloidal stable and well-defined sponge-like nanoparticle can be prepared by a low-energy mechanical method, thanks to the stabilization provided by P80. These nanoparticles have a size of about 100−250 nm with disordered inner structure and large water pores, which can be identified by cryo-TEM and reach up to 13 nm in diameter. The fact that these nanoparticle dispersions have the same large water channels as the corresponding bulk phase; their high stability, and the fact that they are formed of food ingredients, make them promising vehicles for large molecules in a range of applications. This includes (membrane) protein crystallization, enzyme immobilization, or delivery of nutrients and drugs.

ASSOCIATED CONTENT

Supporting Information

The Supporting Information is available free of charge on the ACS Publications website at DOI: 10.1021/acs.langmuir.6b01356.

Equation nonpolar volume fraction; photograph taken of samples between crossed polarizers depicting the dilution line of DGMO/GMO-50 70/30; *Pn*3*m* and L3 SAXS

DOI: 10.1021/acs.langmuir.6b01356
Langmuir 2016, 32, 8650−8659

diffractograms of DGMO/GMO-50/water system; overlapped SAXS profiles from Figure 3 with 50 and 60 wt % water; cryo-SEM picture of sample shown in Figure 4; Fitting swelling laws figures for both cubic phases; densities, A0, and χ values used; estimated D_w; and DLS results (PDF)

AUTHOR INFORMATION

Corresponding Author

*E-mail: maria.valldeperas@fkem1.lu.se.

Notes

The authors declare no competing financial interest.

ACKNOWLEDGMENTS

The research leading to these results has received funding from the People Programme (Marie Curie Actions) of the European Union's Seventh Framework Programme FP7/2007-2013/ under REA grant agreement n° 606713. The authors thank the Swedish synchrotron X-ray facility MAX-IV for allocating beamtime at the I911-4 beamline and Ana Labrador and Sebastian Lages for their support during the measurements. The electron microscopy work was performed at Technion Laboratory for Electron Microscopy of Soft Matter, support by the Technion Russell Berrie Nanotechnology Institute (RBNI). We gratefully acknowledge Yeshayahu Talmon for his expert advice, guidance and valuable discussion on the cryo-EM work.

ABBREVIATIONS

P80, Polysorbate 80; DGMO, diglycerol monooleate; GMO-50, Capmul GMO-50; NPs, nanoparticles; DLS, dynamic light scattering; cryo-TEM, cryogenic transmission electron microscopy; cryo-SEM, cryogenic scanning electron microscopy; SAXS, small angle X-ray scattering; LC, liquid crystalline; L_α, lamellar phase; L_3, sponge phase; Q^{230}, cubic phase with *Ia3d* space group; Q^{224}, cubic phase with *Pn3m* space group; H_2, reverse hexagonal phase; L_2, reverse micellar phase; r_w, water channel radius; D_w, water channel diameter

REFERENCES

(1) Clogston, J.; Rathman, J.; Tomasko, D.; Walker, H.; Caffrey, M. Phase Behavior of a Monoacylglycerol: (Myverol 18−99K)/water System. *Chem. Phys. Lipids* **2000**, *107* (2), 191−220.

(2) Larsson, K. Lipids—Molecular Organization, Physical Functions and Technical Applications. In *The Oily Press*; Taylor & Francis Group: 1994; Vol. *16*, pp 295−295.

(3) Sagalowicz, L.; Leser, M. E.; Watzke, H. J.; Michel, M. Monoglyceride Self-Assembly Structures as Delivery Vehicles. *Trends Food Sci. Technol.* **2006**, *17* (5), 204−214.

(4) Luzzati, V. Biological Significance of Lipid Polymorphism: The Cubic Phases. *Curr. Opin. Struct. Biol.* **1997**, *7* (5), 661−668.

(5) Lindblom, G.; Rilfors, L. Nonlamellar Phases Formed by Membrane Lipids. *Adv. Colloid Interface Sci.* **1992**, *41*, 101−125.

(6) Landh, T. From Entangled Membranes to Eclectic Morphologies: Cubic Membranes as Subcellular Space Organizers. *FEBS Lett.* **1995**, *369* (1), 13−17.

(7) Hyde, S. T.; Schröder, G. E. Novel Surfactant Mesostructural Topologies: Between Lamellae and Columnar (Hexagonal) Forms. *Curr. Opin. Colloid Interface Sci.* **2003**, *8* (1), 5−14.

(8) Lutton, E. Phase Behavior of Aqueous Systems of Monoglycerides. *J. Am. Oil Chem. Soc.* **1965**, *42* (12), 1068−1070.

(9) Hyde, S. T.; Andersson, S.; Ericsson, B.; Larsson, K. A Cubic Structure Consisting of a Lipid Bilayer Forming an Infinite Periodic Minimum Surface of the Gyroid Type in the Glycerolmonooleat-Water System. *Zeitschrift für Krist.* **1984**, *168* (1−4), 213−219.

(10) Johnsson, M.; Lam, Y.; Barauskas, J.; Tiberg, F. Aqueous Phase Behavior and Dispersed Nanoparticles of Diglycerol Monooleate/glycerol Dioleate Mixtures. *Langmuir* **2005**, *21* (11), 5159−5165.

(11) Pitzalis, P.; Monduzzi, M.; Krog, N.; Larsson, H.; Ljusberg-Wahren, H.; Nylander, T. Characterization of the Liquid−Crystalline Phases in the Glycerol Monooleate/Diglycerol Monooleate/Water System. *Langmuir* **2000**, *16* (15), 6358−6365.

(12) Mele, S.; Murgia, S.; Caboi, F.; Monduzzi, M. Biocompatible Lipidic Formulations: Phase Behavior and Microstructure. *Langmuir* **2004**, *20* (13), 5241−5246.

(13) Tran, N.; Hawley, A. M.; Zhai, J.; Muir, B. W.; Fong, C.; Drummond, C. J.; Mulet, X. High-Throughput Screening of Saturated Fatty Acid Influence on Nanostructure of Lyotropic Liquid Crystalline Lipid Nanoparticles. *Langmuir* **2016**, *32* (18), 4509−4520.

(14) Barauskas, J.; Johnsson, M.; Joabsson, F.; Tiberg, F. Cubic Phase Nanoparticles (Cubosome): Principles for Controlling Size, Structure, and Stability. *Langmuir* **2005**, *21* (6), 2569−2577.

(15) Drummond, C. J.; Fong, C. Surfactant Self-Assembly Objects as Novel Drug Delivery Vehicles. *Curr. Opin. Colloid Interface Sci.* **1999**, *4* (6), 449−456.

(16) Larsson, K. Aqueous Dispersions of Cubic Lipid−water Phases. *Curr. Opin. Colloid Interface Sci.* **2000**, *5* (1−2), 64−69.

(17) Mulet, X.; Boyd, B. J.; Drummond, C. J. Advances in Drug Delivery and Medical Imaging Using Colloidal Lyotropic Liquid Crystalline Dispersions. *J. Colloid Interface Sci.* **2013**, *393*, 1−20.

(18) Wadsäter, M.; Barauskas, J.; Nylander, T.; Tiberg, F. Formation of Highly Structured Cubic Micellar Lipid Nanoparticles of Soy Phosphatidylcholine and Glycerol Dioleate and Their Degradation by Triacylglycerol Lipase. *ACS Appl. Mater. Interfaces* **2014**, *6* (10), 7063−7069.

(19) Barauskas, J.; Cervin, C.; Jankunec, M.; Spandyreva, M.; Ribokaite, K.; Tiberg, F.; Johnsson, M. Interactions of Lipid-Based Liquid Crystalline Nanoparticles with Model and Cell Membranes. *Int. J. Pharm.* **2010**, *391* (1−2), 284−291.

(20) Merclin, N.; Bender, J.; Sparr, E.; Guy, R. H.; Ehrsson, H.; Engström, S. Transdermal Delivery from a Lipid Sponge Phase–Iontophoretic and Passive Transport in Vitro of 5-Aminolevulinic Acid and Its Methyl Ester. *J. Controlled Release* **2004**, *100* (2), 191−198.

(21) Guo, C.; Wang, J.; Cao, F.; Lee, R. J.; Zhai, G. Lyotropic Liquid Crystal Systems in Drug Delivery. *Drug Discovery Today* **2010**, *15* (23−24), 1032−1040.

(22) Caffrey, M. A Lipid's Eye View of Membrane Protein Crystallization in Mesophases. *Curr. Opin. Struct. Biol.* **2000**, *10* (4), 486−497.

(23) Wöhri, A. B.; Johansson, L. C.; Wadsten-Hindrichsen, P.; Wahlgren, W. Y.; Fischer, G.; Horsefield, R.; Katona, G.; Nyblom, M.; Oberg, F.; Young, G.; Cogdell, R. J.; Fraser, N. J.; Engström, S.; Neutze, R. A Lipidic-Sponge Phase Screen for Membrane Protein Crystallization. *Structure* **2008**, *16* (7), 1003−1009.

(24) Conn, C. E.; Drummond, C. J. Nanostructured Bicontinuous Cubic Lipid Self-Assembly Materials as Matrices for Protein Encapsulation. *Soft Matter* **2013**, *9* (13), 3449.

(25) Razumas, V.; Kanapieniene, J.; Nylander, T.; Engström, S.; Larsson, K. Electrochemical Biosensors for Glucose, Lactate, Urea, and Creatinine Based on Enzymes Entrapped in a Cubic Liquid Crystalline Phase. *Anal. Chim. Acta* **1994**, *289* (2), 155−162.

(26) Anderson, D.; Wennerstrom, H.; Olsson, U. Isotropic Bicontinuous Solutions in Surfactant-Solvent Systems: The L3 Phase. *J. Phys. Chem.* **1989**, *93* (10), 4243−4253.

(27) Alfons, K.; Engström, S. Drug Compatibility with the Sponge Phases Formed in Monoolein, Water, and Propylene Glycol or Poly(ethylene Glycol). *J. Pharm. Sci.* **1998**, *87* (12), 1527−1530.

(28) Engström, S.; Alfons, K.; Rasmusson, M.; Ljusberg-Wahren, H. Solvent-Induced Sponge (L3) Phases in the Solvent-Monoolein-Water System. *Colloid Sciende of Lipids: New paradigms for sel-assembly in science and technology* **1998**, *108*, 93−98.

(29) Tyler, A. I. I.; Barriga, H. M. G.; Parsons, E. S.; McCarthy, N. L. C.; Ces, O.; Law, R. V.; Seddon, J. M.; Brooks, N. J. Electrostatic

DOI: 10.1021/acs.langmuir.6b01356
Langmuir 2016, 32, 8650−8659

Swelling of Bicontinuous Cubic Lipid Phases. *Soft Matter* **2015**, *11* (16), 3279−3286.
(30) Landh, T. Phase Behavior in the System Pine Needle Oil Monoglycerides-Poloxamer 407-Water at 20°C. *J. Phys. Chem.* **1994**, *98* (34), 8453−8467.
(31) Barauskas, J.; Misiunas, A.; Gunnarsson, T.; Tiberg, F.; Johnsson, M. Sponge" nanoparticle Dispersions in Aqueous Mixtures of Diglycerol Monooleate, Glycerol Dioleate, and Polysorbate 80. *Langmuir* **2006**, *22* (14), 6328−6334.
(32) Sun, W.; Vallooran, J. J.; Zabara, A.; Mezzenga, R. Controlling Enzymatic Activity and Kinetics in Swollen Mesophases by Physical Nano-Confinement. *Nanoscale* **2014**, *6* (12), 6853−6859.
(33) Turner, D. C.; Wang, Z.-G.; Gruner, S. M.; Mannock, D. A.; McElhaney, R. N. Structural Study of the Inverted Cubic Phases of Di-Dodecyl Alkyl-B-D-Glucopyranosyl-Rac-Glycerol. *J. Phys. II* **1992**, *2* (11), 2039−2063.
(34) Anderson, D. M.; Gruner, S. M.; Leibler, S. Geometrical Aspects of the Frustration in the Cubic Phases of Lyotropic Liquid Crystals. *Proc. Natl. Acad. Sci. U. S. A.* **1988**, *85* (15), 5364−5368.
(35) Briggs, J.; Chung, H.; Caffrey, M. The Temperature-Composition Phase Diagram and Mesophase Structure Characterization of theMonoolein/Water System. *J. Phys. II* **1996**, *6* (5), 723−751.
(36) Danino, D. Cryo-TEM of Soft Molecular Assemblies. *Curr. Opin. Colloid Interface Sci.* **2012**, *17* (6), 316−329.
(37) Danino, D.; Bernheim-Groswasser, A.; Talmon, Y. Digital Cryogenic Transmission Electron Microscopy: An Advanced Tool for Direct Imaging of Complex Fluids. *Colloids Surf., A* **2001**, *183−185*, 113−122.
(38) Holstborg, J.; Pedersen, B.; Krog, N.; Olesen, S. Physical Properties of Diglycerol Esters in Relation to Rheology and Stability of Protein-Stabilised Emulsions. *Colloids Surf., B* **1999**, *12* (3−6), 383−390.
(39) Roux, D.; Cates, M. E.; Olsson, U.; Ball, R. C.; Nallet, F.; Bellocq, A. M. Light Scattering from a Surfactant "Sponge" Phase: Evidence for a Hidden Symmetry. *Europhys. Lett.* **1990**, *11* (3), 229−234.
(40) Lei, N.; Safinya, C. R.; Roux, D.; Liang, K. S. Synchrotron X-Ray-Scattering Studies on the Sodium Dodecyl Sulfate−water−pentanol−dodecane L 3 Sponge Phase. *Phys. Rev. E: Stat. Phys., Plasmas, Fluids, Relat. Interdiscip. Top.* **1997**, *56* (1), 608−613.
(41) Angelov, B.; Angelova, A.; Mutafchieva, R.; Lesieur, S.; Vainio, U.; Garamus, V. M.; Jensen, G. V.; Pedersen, J. S. SAXS Investigation of a Cubic to a Sponge (L3) Phase Transition in Self-Assembled Lipid Nanocarriers. *Phys. Chem. Chem. Phys.* **2011**, *13* (8), 3073−3081.
(42) Murgia, S.; Falchi, A. M.; Mano, M.; Lampis, S.; Angius, R.; Carnerup, A. M.; Schmidt, J.; Diaz, G.; Giacca, M.; Talmon, Y.; Monduzzi, M. Nanoparticles from Lipid-Based Liquid Crystals: Emulsifier Influence on Morphology and Cytotoxicity. *J. Phys. Chem. B* **2010**, *114* (10), 3518−3525.
(43) Siegel, D. P. Inverted Micellar Intermediates and the Transitions between Lamellar, Cubic, and Inverted Hexagonal Amphiphile Phases. III. Isotropic and Inverted Cubic State Formation via Intermediates in Transitions between Lα and HII Phases. *Chem. Phys. Lipids* **1986**, *42* (4), 279−301.
(44) Siegel, D. P. The Modified Stalk Mechanism of Lamellar/Inverted Phase Transitions and Its Implications for Membrane Fusion. *Biophys. J.* **1999**, *76* (1), 291−313.
(45) Efrat, R.; Kesselman, E.; Aserin, A.; Garti, N.; Danino, D. Solubilization of Hydrophobic Guest Molecules in the Monoolein Discontinuous Q_L Cubic Mesophase and Its Soft Nanoparticles. *Langmuir* **2009**, *25* (3), 1316−1326.
(46) Wadsäter, M.; Barauskas, J.; Rogers, S.; Skoda, M. W. a.; Thomas, R. K.; Tiberg, F.; Nylander, T. Structural Effects of the Dispersing Agent Polysorbate 80 on Liquid Crystalline Nanoparticles of Soy Phosphatidylcholine and Glycerol Dioleate. *Soft Matter* **2015**, *11* (6), 1140−1150.

DOI: 10.1021/acs.langmuir.6b01356
Langmuir 2016, 32, 8650−8659